

Multigroup discrete ordinates modeling of ^{125}I 6702 seed dose distributions using a broad energy-group cross section representation

George M. Daskalov^{a)}

National Research Council of Canada, IRS/INMS, 1500 Montreal Road, Ottawa ON K1A 0R6, Canada

R. S. Baker

Los Alamos National Laboratory, MS D409, Los Alamos, New Mexico 87545

D. W. O. Rogers

National Research Council of Canada, IRS/INMS, 1500 Montreal Road, Ottawa ON K1A 0R6, Canada

J. F. Williamson

Washington University Medical School, Radiation Oncology Physics, 510 S. Kingshighway Boulevard, St. Louis, Missouri 63110

(Received 19 March 2001; accepted for publication 31 October 2001; published 9 January 2002)

Our purpose in this work is to demonstrate that the efficiency of dose-rate computations in ^{125}I brachytherapy, using multigroup discrete ordinates radiation transport simulations, can be significantly enhanced using broad energy group cross sections without a loss of accuracy. To this end, the DANTSYS multigroup discrete ordinates neutral particle transport code was used to estimate the absorbed dose-rate distributions around an ^{125}I -model 6702 seed in two-dimensional (2-D) cylindrical R-Z geometry for four different problems spanning the geometries found in clinical practice. First, simulations with a high resolution 210 energy groups library were used to analyze the photon flux spectral distribution throughout this set of problems. These distributions were used to design an energy group structure consisting of three broad groups along with suitable weighting functions from which the three-group cross sections were derived. The accuracy of 2-D DANTSYS dose-rate calculations was benchmarked against parallel Monte Carlo simulations. Ray effects were remedied by using the DANTSYS internal first collision source algorithm. It is demonstrated that the ^{125}I primary photon spectrum leads to inappropriate weighting functions. An accuracy of $\pm 5\%$ is achieved in the four problem geometries considered using geometry-independent three-group libraries derived from either material-specific weighting functions or a single material-independent weighting function. Agreement between Monte Carlo and the three-group DANTSYS calculations, within three standard Monte Carlo deviations, is observed everywhere except for a limited region along the Z axis of rotational symmetry, where ray effects are difficult to mitigate. The three-group DANTSYS calculations are 10–13 times faster than ones with a 210-group cross section library for ^{125}I dosimetry problems. Compared to 2-D EGS4 Monte Carlo calculations, the 3-group DANTSYS simulations are a 100-fold more efficient. Provided that these efficiency gains can be sustained in three-dimensional geometries, the results suggest that discrete ordinates simulations may have the potential to serve as an efficient and accurate dose-calculation algorithm for low-energy brachytherapy treatment planning. © 2002 American Association of Physicists in Medicine.

[DOI: 10.1118/1.1429238]

Key words: multigroup discrete ordinates photon transport, Monte Carlo photon transport, photon kerma, absorbed dose, I-125 6702 seed, brachytherapy dosimetry

I. INTRODUCTION

The Discrete Ordinates Method (DOM) is a deterministic solution of the general Boltzmann equation governing particle transport. DOM replaces the continuous energy, angle, and spatial variables of the transport equation with discrete bins, over which the photon flux and derived quantities (e.g., dose) are averaged. The energy variable is discretized by means of the multigroup energy approach using precalculated multigroup cross section libraries. For discretization of the spatial and angular variables, finite-difference and collocation schemes are employed. The original equation is replaced by a series of simultaneous linear difference equations

that are solved iteratively. A simplified derivation of the multigroup energy approach and the spatial and angular discretizations involved can be found in our previous work.¹ A more general derivation can be found in the textbook by Lewis and Miller² and in the references therein. The solution of discrete ordinates equations approaches the exact solution of the Boltzmann equation as the space, energy, and angle discrete bin sizes approach differential size.

A typical ^{125}I brachytherapy problem consists of a number of Ti-encapsulated ^{125}I sources implanted in or near localized tumors. The photoelectric effect, together with the coherent and incoherent scattering, are the prevalent photon interac-

tion processes in this energy range (below 36 keV). Because of the photoelectric effect, the total interaction cross section varies rapidly with energy and changes significantly with the atomic number of the medium. As a result, even relatively small changes in the tissue composition and density can significantly perturb the administered dose distribution.^{3,4} Our previous work^{1,5,6} has demonstrated that the DANTSYS discrete ordinates code system⁷ can accurately (within 2%–3%) reproduce dose distributions derived from Monte Carlo photon transport simulations for encapsulated sources throughout the brachytherapy energy range. This work established the range of DANTSYS user code parameters and other conditions needed to achieve such accuracy. One such condition is the suitability of the multigroup library used. Our previous studies^{1,6} used a high-resolution 210-energy group cross-section library (referred to below as G-210), which produces accurate results but achieves limited efficiency gains in comparison with Monte Carlo simulations.

The main goals of this study are (1) to develop broad energy–group cross section libraries containing the smallest possible number of energy groups for ¹²⁵I brachytherapy; (2) to demonstrate that a single precalculated, geometry-independent broad energy–group library exists that sustains acceptable dose-calculation accuracy over a broad range of clinically relevant problem geometries; and (3) to demonstrate the potential for efficiency gains by reducing the number of energy groups used. For these purposes, we employ DANTSYS in conjunction with the G-210 to obtain the photon flux spectra and dose distributions around the ¹²⁵I Model 6702 seed. The spectral data are used to derive energy-dependent weighting functions from which to develop broad energy–group cross-section libraries. The accuracy of the DANTSYS calculations is evaluated by comparison to continuous energy Monte Carlo simulations. Finally, we demonstrate the efficiency of the broad energy–group DOM calculations relative to DOM with G-210 and in comparison with two-dimensional EGS4 Monte Carlo simulations.

II. MATERIALS AND METHODS

A. The theory of the multigroup energy approximation

The multigroup energy approximation in radiation transport² assumes that the energy domain $(0, E_0)$ is partitioned into G intervals of width $\Delta E_g = E_g - E_{g+1}$, for $g = 1, \dots, G$. By convention the energy decreases with increasing group number. Thus, $E_1 = E_0$, the maximum energy of photons emitted by the sources, and $E_{G+1} = 0$. The photons within group g are taken to be just those with energy between E_g and E_{g+1} . By averaging all quantities characterizing the problem (e.g., particle fluxes and interaction cross sections) over each energy group, they become functions of the group index, g , rather than energy, E . Within the framework of the theory of the multigroup approximation, the group averaged total cross sections $\mu_{t,g}(\mathbf{r})$ can be obtained as²

$$\mu_{t,g}(\mathbf{r}) = \frac{\int_{\Delta E_g} \mu_t(\mathbf{r}, E) \Phi(\mathbf{r}, E) dE}{\Phi_g(\mathbf{r})}, \quad (1)$$

where $\mu_t(\mathbf{r}, E)$ is the continuous energy total cross section, and $\Phi(\mathbf{r}, E)$ is the scalar flux (distribution of the particle fluence with respect to energy in the ICRU nomenclature⁸). The quantity $\Phi_g(\mathbf{r})$ is the group scalar flux corresponding to $\Phi(\mathbf{r}, E)$,

$$\Phi_g(\mathbf{r}) = \int_{\Delta E_g} \Phi(\mathbf{r}, E) dE. \quad (2)$$

In practice, group cross sections are calculated by means of an approximation to the actual, problem-dependent, and generally unknown, scalar flux, known as the spectral weighting function $f(E)$. Most commonly, energy separability is assumed,² i.e.,

$$\Phi(\mathbf{r}, E) \approx f(E) \cdot \Phi_g(\mathbf{r}), \quad E_{g+1} \leq E < E_g. \quad (3)$$

Substituting Eq. (3) into Eq. (1) and using Eq. (2), the resulting group cross section, $\mu_{t,g}(\mathbf{r})$, becomes

$$\mu_{t,g}(\mathbf{r}) = \frac{\int_{\Delta E_g} \mu_t(\mathbf{r}, E) f(E) dE}{\int_{\Delta E_g} f(E) dE}. \quad (4)$$

Expressions similar to (4) can be derived for other types of interaction cross sections.^{1,2,9} In general, as the energy bins widen, the dependency of $f(E)$, the resulting multigroup cross sections, and DOM accuracy on the particular problem geometry increase. Conversely, as the energy bin widths approach zero, the multigroup constants approach the corresponding pointwise values and become independent of the choice of $f(E)$.

G-210 has very narrow energy bins (less than 2 keV wide below 100 keV), allowing the use of an energy-independent, constant weighting function. Thus G-210 simulations do not depend on the particular shape of the photon spectrum in a given system and are “application independent.” In addition, due to the high energy resolution, such simulations can provide detailed photon spectral distributions throughout the simulated system. However, the large number of energy groups leads to highly CPU intensive calculations.^{1,6} The computational efficiency of DOM calculations is roughly proportional to the number of phase space cells, which, in turn, is proportional to the number of energy groups used in the calculations. The use of broader energy bins and a correspondingly smaller number of groups is an important step toward increasing the computational efficiency of DOM calculations.

We hypothesize that broad energy–group libraries, based upon a small number of groups and appropriate weighting functions, can be developed that maintain acceptable accuracy over a broad range of ¹²⁵I brachytherapy problem geometries. The NJOY nuclear data processing system⁹ was used to develop a set of broad three-group cross section libraries with weighting functions derived from the photon spectral information obtained by DANTSYS G-210 calculations. Four single-seed problem geometries, encompassing a wide range of material compositions and problem geometries

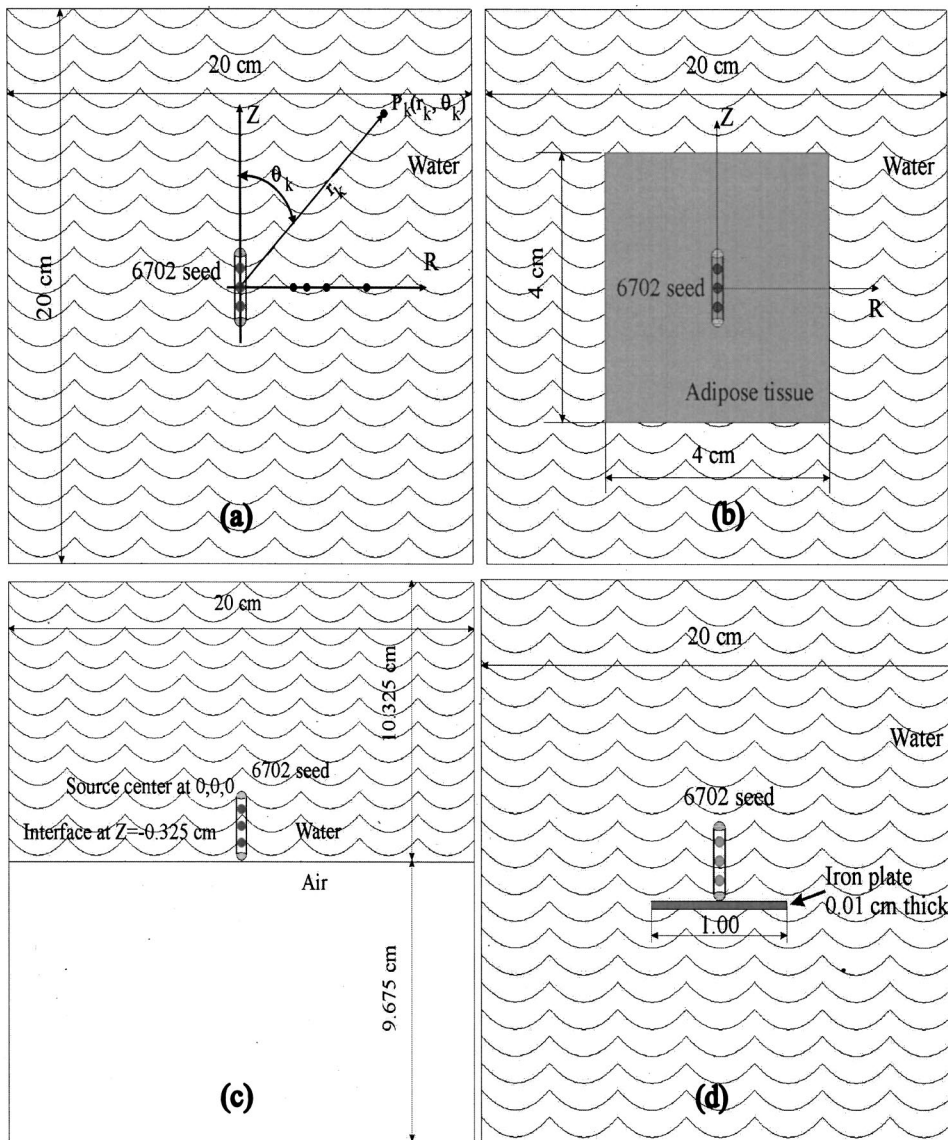


FIG. 1. Geometry and composition of the problems: (a) Problem 1—homogeneous water phantom; an estimator point P_k with its polar coordinates (r_k, θ_k) is also shown. (b) Problem 2—the seed embedded in a 4 cm \times 4 cm adipose tissue cylinder in the water phantom from (a) adipose tissue (ICRU-44) by weight—1.14% H, 59.8% C, 0.7% N, 27.8% O, 0.1% Na, 0.1% S, 0.1% Cl, with density $\rho = 0.95 \text{ g cm}^{-3}$. (c) Problem 3—Air-water interface problem; air by weight—75.53% N, 23.18% O, 1.29% Ar, with a density of $\rho = 1.20 \times 10^{-3} \text{ g cm}^{-3}$. (d) Problem 4—Iron disk (density $\rho = 7.874 \text{ g cm}^{-3}$) of thickness 0.01 cm and diameter 1 cm under the seed in the water phantom from (a).

encountered in brachytherapy clinical practice, were designed (cf. Sec. II B). To evaluate a given broad energy-group cross-section library, DANTSYS calculations were compared to continuous-energy Monte Carlo photon transport simulations of the absorbed dose rates per unit contained activity throughout the problems described above. These Monte Carlo results are used as a “gold standard” to evaluate the accuracy of the corresponding DANTSYS calculations with a given cross-section library.

B. The benchmark problems

Figure 1 illustrates the four problem geometries selected for our study. Figure 1(a) shows *Problem 1*: a cylindrical water phantom of diameter 20 cm and height 20 cm with a model 6702 ^{125}I seed at its center. This approximates the reference conditions assumed by the single-source dose-rate distributions recommended by the TG-43 clinical protocol.¹⁰ *Problem 2* [Fig. 1(b)]: consists of a 6702 seed at the center of a 4 cm diam and 4 cm height adipose tissue cylinder embed-

ded in the larger cylindrical water phantom of problem 1. This geometry approximates implanting seeds in a fat-like tissue. *Problem 3* [Fig. 1(c)] consists of a cylindrical phantom of diameter 20 cm and height 20 cm. Here 10.325 cm of its height is filled with water while the remaining volume contains air. In clinical practice, such geometry might be encountered when a superficial tumor, near the tissue-air interface, is implanted. A model 6702 seed is embedded in the water part with its center at a depth of 0.325 cm from the water air interface. *Problem 4* [Fig. 1(d)] differs from problem 1 by the presence of an iron disk of diameter 1 cm and thickness 0.01 cm (approximately 1 mean-free path of a photon with an average ^{125}I source energy of 28.33 keV). Clinically, this geometry approximates the use of ^{125}I in episcleral eye-plaque therapy or placement of seeds near a metal prosthesis. The absorbed dose rate was evaluated only in water and in adipose tissue media of problems 1–4 as the dose delivered to foreign metal bodies and air is of no clinical relevance.

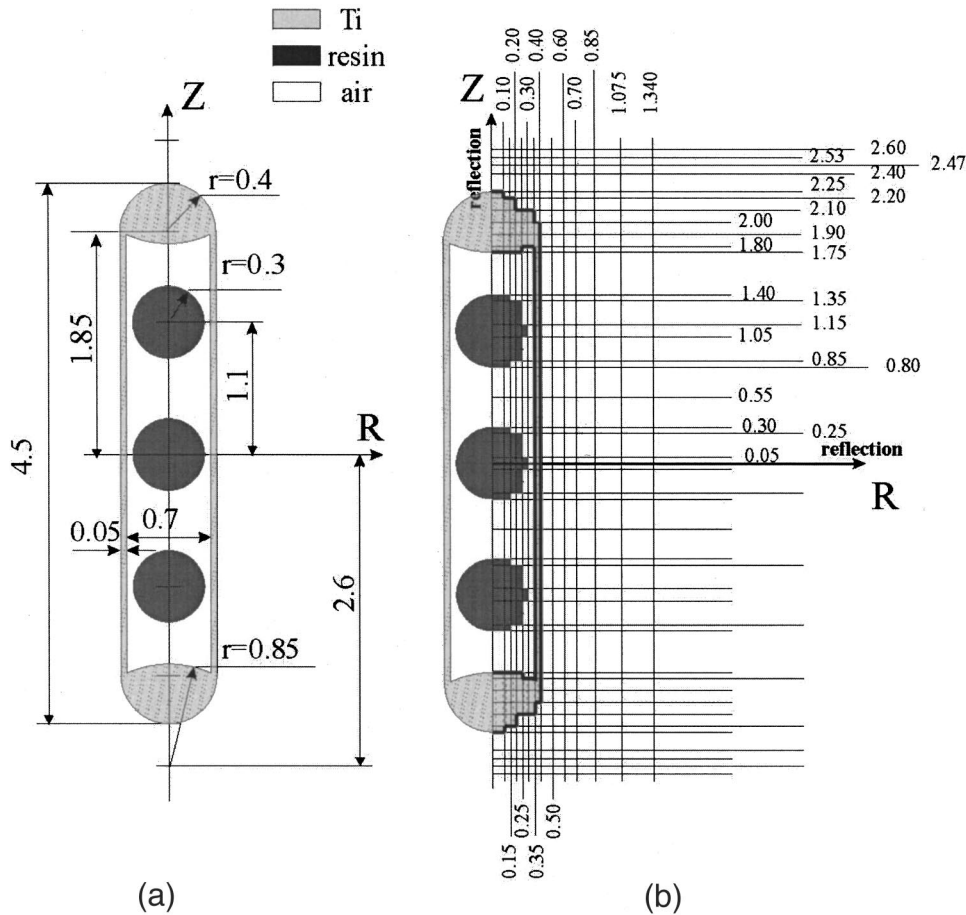


FIG. 2. The geometry representation of the ^{125}I 6702 seed by the MCPT (a) and DANTSYS (b). Material composition: ion-exchange resin ($\text{C}_{12}\text{H}_{18}\text{NCl}$) spheres (density $\rho = 1.2 \text{ g cm}^{-3}$) with uniformly distributed ^{125}I throughout their volume; Ti capsule ($\rho = 4.54 \text{ g cm}^{-3}$); air with composition by weight—75.53% N, 23.18% O, 1.29% Ar, with density $\rho = 1.20 \times 10^{-3} \text{ g cm}^{-3}$. All dimensions are in mm.

C. Computational details

1. Monte Carlo calculations

The continuous energy Monte Carlo Photon Transport MCPT code,^{3,4,11–15} PTRAN_CCG (Version 7.42) developed in our laboratory was used to calculate the benchmark dose distributions. Incoherent and coherent scattering, together with the photoelectric effect, were simulated in all calculations. Characteristic x-ray production, however, was suppressed since it is not modeled by our multigroup DOM calculations. The macroscopic cross sections, as well as the normalized probabilities for the various photon interaction types, were derived from the DLC-146 cross-section library.¹⁶ The code is equipped with a geometric modeling system that allows complex objects to be described as set-theoretic unions, intersections, and differences of simple convex regions. MCPT neglects the secondary electrons liberated by the photon interactions. Instead, the mass energy absorption coefficients of Hubbell and Seltzer¹⁷ were used to convert the photon energy flux into collision kerma. Due to negligible attenuation (0.014%) of 28.3 keV photons over the $3.2 \mu\text{m}$ range of secondary electrons liberated, secondary charged particle equilibrium is known to exist with a high degree of accuracy.¹⁸ Thus, an absorbed dose can be accurately approximated by collision kerma^{11,18} except within a few microns of any tissue–metal interface.

The seed geometry model of the ^{125}I model 6702 used is the same as described by Williamson¹⁹ and is shown in Fig. 2(a). The bounded next flight estimator technique¹² was used to evaluate the dose rates $\dot{D}(r, \theta)$ at various points $P_k(r_k, \theta_k)$ [see Fig. 1(a) for an illustration of the polar coordinate system] in water and adipose tissue surrounding the ^{125}I seed. Angular dose-rate profiles $\dot{D}(r, \theta)$ for θ (0° – 180°) were evaluated at $r = 0.25, 0.5, 1, 3,$ and 5 cm as well as the radial distribution ($\theta = 90^\circ$) for r in the range 0.1 – 7 cm . Depending on distance, between 500 000 and 6 500 000 histories were analyzed, leading to maximum standard errors of the mean (67% confidence interval) ranging from 0.4% (at 0.25 cm distance) to 1.35% (at 7 cm). Only for a single estimator point adjacent to the iron disk (problem 4) and for 5 estimator points beyond 5 cm distance from the seed center in each problem, the standard error of the mean was larger, reaching 2.5%. The MCPT dose rates had units of cGy/mCi h and used in this form to evaluate DANTSYS accuracy ($1 \text{ cGy mCi}^{-1} \text{ h}^{-1} = 7.508 \times 10^{-1} \text{ Gy Bq}^{-1} \text{ s}^{-1}$). The ^{125}I photon source spectrum used is the one given by NCRP.²⁰ Hereafter we refer to the results of PTRAN_CCG calculations as “MCPT simulations.”

Our MCPT simulations are an unbiased and rigorous benchmark for assessing the accuracy of DANTSYS calculations. However, the PTRAN_CCG code is fully three dimensional and unable to exploit the cylindrical symmetry of the

problem. Thus, to provide a Monte Carlo efficiency benchmark with spatial dimensionality equivalent to our DANTSYS 2-D calculations, we used the EGS4 user code DOSRZ²¹ in 2-D cylindrical R-Z geometry using the same spatial cells as in DANTSYS calculations. We emphasize that DOSRZ was used solely to evaluate the relative efficiency of DANTSYS.^{1,6} DOSRZ accommodates the R-Z geometry by scoring the energy deposited in circular rings with intersections corresponding to the DANTSYS R-Z grid [Fig. 2(b)] with no variance reduction techniques applied. Secondary electron transport was suppressed to avoid unnecessary calculations. The number of histories was selected to achieve a maximum standard error of the mean of about 2.5% in 99% of the volume elements in a 20 cm diam by 20 cm height scoring grid, except for problem 3, where scoring was limited to the water-filled fraction of the overall phantom.

2. DANTSYS multigroup discrete ordinates calculations

The DANTSYS code package⁷ is a modular computer program designed to solve the time-dependent, multigroup linear transport equation in several different geometries using the discrete ordinates method. The TWODANT module solves the two-dimensional transport equation iteratively using the diamond differencing or adaptive weighted diamond differencing (AWDD) method²² for space/angle discretization. The diffusion synthetic acceleration (DSA) method²³ is used to accelerate the convergence of the solution iteration process.

The TWODANT module was used to solve the photon transport problem for geometries 1–4 (Fig. 1) in two-dimensional cylindrical R-Z geometry. The finite-difference spatial mesh used to describe the source geometry is shown in Fig. 2(b). A reflective boundary condition⁷ was assumed along the Z axis of source rotational symmetry, together with vacuum boundary conditions along the outer surface of the modeled phantoms. The symmetry with respect to the transverse seed plane in problems 1 and 2 allowed the application of a reflective boundary condition along it, thus reducing the analyzed volume to 1/2. We note that the use of such a boundary condition is not necessary and is suitable only for highly idealized problems. Variable voxel sizes, all smaller than 0.5 mean-free paths (mfp) along the R axis, were used. Small voxel sizes were needed to model the source geometry accurately (less than 0.1 mfp in the vicinity and inside the source). The ratio of the Z axis to R axis voxel dimensions (the aspect ratio) varied from 2:1 near the source volume to 15:1 at the periphery of the water phantom in the vicinity of the R or Z axis. In all problems, the seed geometry and composition used was the same as in Fig. 2(b). The finite-difference approximation for the rest of the geometry was problem dependent. The resulting voxel structure contained 63 (along the R axis) by 61 (along the Z axis) voxels for problems 1 and 2, 73 by 10 for problem 3, and 68 by 122 voxels for problem 4. Similar to our previous work,^{1,5,6} the adaptive weighted diamond differencing method was used to eliminate negative flux fixups.

Quadrature sets containing 36 (denoted as S_{16}), 55 (S_{20}),

91 (S_{26}), 120 (S_{30}), and 171 (S_{36}) angular directions and corresponding weights per octant were used for angular discretization in order to evaluate the effect of quadrature on DANTSYS accuracy.

In two- and three-dimensional geometries, the streaming of the particles along discrete angular directions leads to artificial fluctuations of the flux known as ray effects.^{1,2} Similar to our previous studies,^{1,6} we used TWODANT's ray-tracing first collision source option²⁴ to mitigate the ray effects. Up to 399 000 ray-tracing histories were used to create the first collision source.

All multigroup libraries were derived from the same continuous-energy cross section library, DLC-146, used by the MCPT simulations. The three-group libraries as well as G-210 contain the scattering cross section matrix coefficients allowing up to fifth degree (P_5) Legendre polynomial expansion of the cross section angular dependency.² Following the results in our previous work,^{1,6} we used P_3 angular polynomial expansion for all calculations.

The multigroup approximation of the ^{125}I polychromatic spectrum and the appropriate normalization was determined using the procedure described in our previous work.⁵ The highest energy of ^{125}I photons appears in the 126th group of G-210 and hence the solution spanned 85 groups, starting with group 126. The remaining computational parameters used were the same as in our previous work.^{1,6}

At the conclusion of each DANTSYS calculation, the DANTSYS EDIT module⁷ was employed to convert the flux distributions into absorbed dose rate by using the group kerma factors included in each multigroup set. Under the condition of secondary charged particle equilibrium, and the lack of bremsstrahlung in water for ^{125}I energies, the collision kerma is essentially equivalent to kerma and both accurately approximate the absorbed dose.^{1,6} The DANTSYS EDIT results were utilized in the form of two-dimensional arrays of absorbed dose rates at points centered at each voxel of the finite-difference geometry approximation. A bilinear interpolation procedure^{1,6} utilizing the Task Group 43 geometry factor $G(r, \theta)$ ¹⁰ to suppress spatial flux variations due to inverse square law, was used to obtain DANTSYS estimates at points not coinciding with any of the spatial grid points.

D. The development of three-group libraries

Three energy groups were derived subject to the following constraints: the energy range of the three-group bins is 1–35.5 keV; the first group (27.0–35.5 keV) include all primary ^{125}I photon energies; the photon flux represented by the third and lowest-energy group (1–16.9 keV) is at least ten orders of magnitude less than the first group flux according to the G-210 DANTSYS simulations of problem 1.

The three-group energy bin structure is shown in Table I.

We developed an automated procedure for generating weighting functions based on the spectral information provided by the G-210 DANTSYS simulations. First, we obtain the photon spectrum, as a function of the G-210 group index, g , at each point $P(r, \theta)$:

TABLE I. The energy group boundaries of the three-group libraries used in this study. The group number increases with energy decreasing.

Group number	Upper energy (keV)	Lower energy (keV)
1	35.50	27.00
2	27.00	16.90
3	16.90	1.00

$$\varphi_g(r, \theta) = \frac{1}{\Delta E_g} \frac{\Phi_g(r, \theta)}{\sum_{g'=1}^G \Phi_{g'}(r, \theta)}, \quad g = 1, \dots, G, \quad (5)$$

where $\Phi_g(r, \theta)$ is the group scalar flux directly obtained from the G-210 DANTSYS calculations at the selected point $P(r, \theta)$. The denominator in Eq. (5) assures that $\sum_{g=1}^G \varphi_g(r, \theta) \Delta E_g = 1$. The finely discretized photon spectrum $\varphi_g(r, \theta)$ is available as a histogram over the corresponding 210-group energy bins. Finally, after choosing a point and fixing its spatial coordinates (r, θ) , the spectral weighting function $f(E)$ [Eq. (4)] is given by

$$f(E) = \varphi_g(r, \theta), \quad \text{if } E \in [E_{g+1}, E_g], \quad g = 126, \dots, 210, \quad (6)$$

where the group index range corresponds to the G-210 groups spanning the 1–35.5 keV energy range.

Several cross-section libraries were developed to investigate the influence of the different weighting functions derived with photon spectra observed in different materials on the accuracy of the DANTSYS calculations. Library G-3a was based upon using different weighting functions for each medium present in the system (*water, resin, adipose, Ti, and Fe*). For each of these media, the reference point (r, θ) was taken near the center of the corresponding material, usually on the transverse axis (see the caption of Fig. 4). Additional libraries, based upon the same three-group energy bins, were developed based upon the following weighting functions.

- (i) G-3b: a 3-group library based upon a material-independent weighting function derived from the photon spectrum in *water*.
- (ii) G-3c: based on a material-independent weighting function derived from the photon spectrum in *Ti*.
- (iii) G-3e: derived from a material-independent weighting function based on the I-125 primary photon spectrum.
- (iv) G-3g: based on a material-independent weighting function derived from the photon spectrum in *Fe*.

The group flux-to-kerma conversion coefficients (group kerma factors) were calculated by NJOY for each three-group library. All libraries used in this study together with their respective names and weighting functions are shown in Table II. The *resin* weighting function was used for air in all cases. For each of these libraries, the total cross sections and kerma factors were evaluated. In addition, the accuracy of DANTSYS calculations was evaluated relative to Monte Carlo calcula-

TABLE II. Multigroup library names and weighting functions used for their development. The weighting function notation used is introduced in Fig. 4.

Library name	Number of groups	Weighting functions used
G-210	210	constant
G-3a	3	Material specific as in Fig. 4
G-3b	3	<i>water</i>
G-3c	3	<i>Ti</i>
G-3e	3	<i>I-125</i>
G-3g	3	<i>Fe</i>

tions for each of the four benchmark-problems and for each three-group library.

III. RESULTS AND DISCUSSION

A. Benchmark geometries

Figure 3 shows the polar dose-rate profiles for the ^{125}I 6702-type seed, as obtained by the MCPT and DANTSYS simulations, at a 1 cm distance from the source for all problems. The large variations in the absorbed dose rates (from 10% in problem 3 to 68% in problem 4) relative to problem 1 are evident in the figure. The figure also demonstrates the excellent agreement between DANTSYS with G-210 and MCPT for all problem geometries and angles shown.

B. Spectral weighting functions and cross-section libraries

Table I lists the boundaries of the G-3 energy group structure. For each of the three-group libraries listed in Table II, Fig. 4 shows the weighting functions derived from the analysis of the G-210 DANTSYS benchmark problem simulations, together with the particular (r, θ) coordinates and material

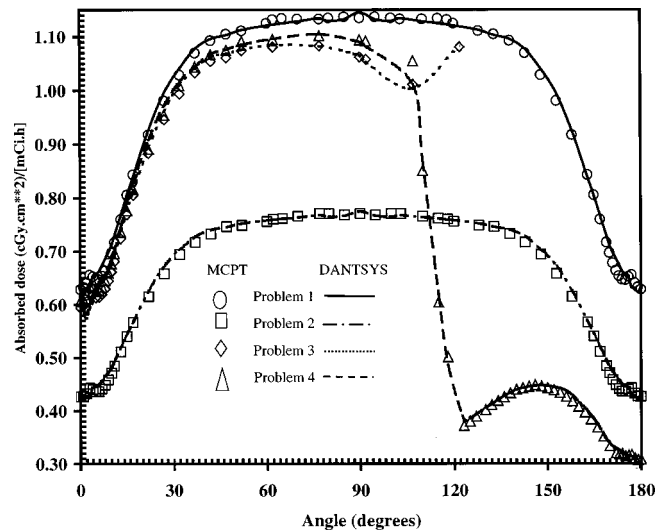


FIG. 3. MCPT (symbols) and DANTSYS (lines) absorbed dose rates multiplied by the distance squared at 1 cm from the source center in the range 0° – 180° , except for problem 3 where the range is 0° – 122° and is determined by the position of the water–air interface. For problem 2 the results represent the dose in the adipose tissue. DANTSYS with G-210 results and S_{16} (problems 1 and 2) and S_{20} (problems 3 and 4).

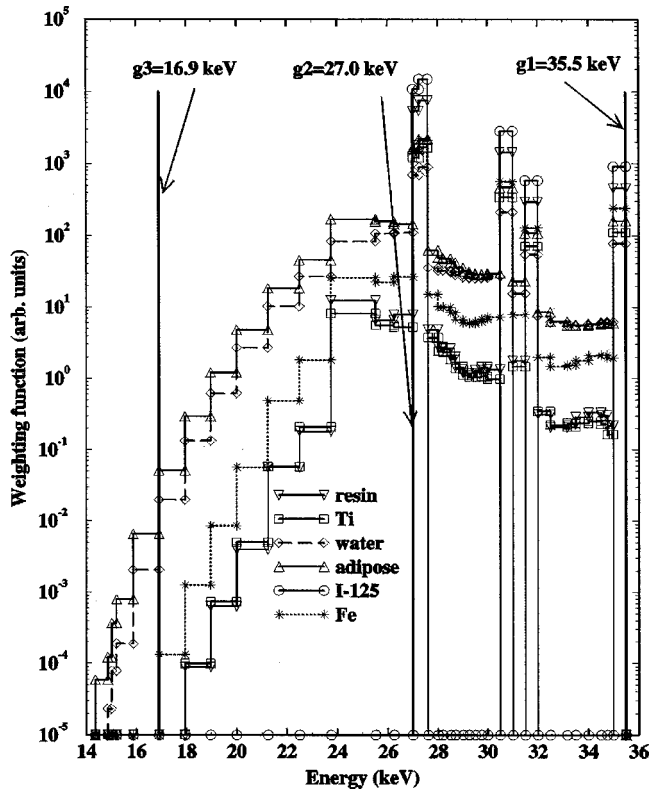


Fig. 4. Weighting functions derived from photon spectra obtained by DANTSYS with G-210. The I-125 denotes a weighting function corresponding to the ^{125}I primary photon spectrum. The *resin* and *Ti* denote weighting functions due to φ_g in resin (at $r=0$ cm) and in the Ti seed tip ($r=0.19$ cm, $\theta=0^\circ$) in problem 1. The *water* refers to a weighting function derived with φ_g at $r=3.07$ cm, $\theta=90^\circ$. The *adipose* denotes a weighting function due to φ_g at $r=156$ cm, $\theta=90^\circ$ (in the adipose tissue fraction of the phantom geometry) in problem 2. *Fe* denotes a function due to φ_g at $r=0.32$ cm, $\theta=137.6^\circ$ in the Fe disk in problem 4. The energies of the three-group boundaries are also shown.

composition where the φ_g is evaluated. Figure 4 also includes a weighting function based on the 210-group approximation of the ^{125}I primary photon spectrum illustrating the G-210 energy bins corresponding to the source photon energies. Note that an energy-independent (constant) weighting function is assumed in the energy range where φ_g is smaller than a selected cut-off value (in our case 10^{-13}). All weighting functions are dominated by the primary photon energies. The largest variations are evident in energy bins that are dominated by geometry- and material-dependent scattered-

photon contributions rather than by primary photons. Because of the nature of the weighting functions and the way the energy group structure was designed, these 3-group cross section libraries are applicable only to problems with ^{125}I primary spectra.

Table III shows the macroscopic group-averaged total cross sections for water, adipose tissue, and titanium for all 3-group libraries. G-3a cross sections coincide with those of G-3b for water and with G-3c cross sections for Ti, since G-3a is developed using the same weighting functions for the respective materials. The cross section magnitudes do not differ by more than 3.8% (the largest difference for Ti) for all libraries in group 1. Similar differences are observed in group 2, except for G-3e, where they exceed 35% thus illustrating the impact of the energy-independent weighting function used in G-3e development for this group. It will be seen later in this study that the large discrepancies in group 3 (generally exceeding a factor of 10) are not important since the photon fluxes in this group have negligible contribution to the dose distribution. Similar conclusions hold for the group kerma factors shown in Table IV.

C. Analysis of the accuracy and efficiency of DANTSYS with the three-group libraries

Figures 5–9 show comparisons of DANTSYS absorbed dose rates in water (Figs. 5, 7, 8, and 9) and adipose tissue (Fig. 6) for problems 1–4, respectively, using various multi-group libraries. The MCPT dose rates at 1 cm for all problems are the ones in Fig. 3. Figure 9 illustrates DANTSYS relative to MCPT dose results as a function of distance from the seed center in the case of problem 4. S_{16} angular quadrature (36 angular directions and weights) is used for problems 1 and 2 (Figs. 5 and 6, respectively) and S_{20} (55 directions and weights) is used for problems 3 and 4 (Figs. 7, 8, and 9). The figures show that DOM simulations with G-3e (primary ^{125}I spectral weighting function in Fig. 4) reproduces the MCPT data less accurately than the other simulations, with differences, in general, exceeding 3%–5% depending on the problem. G-3e tends to overestimate the primary photon contribution to the total dose close to the source (within 0.5 mfp or about 1.1 cm in water for an average primary photon energy of 28.33 keV). At the same time, it underestimates the scattered photon contribution at larger distances. As a result, DANTSYS simulations with G-3e deviate significantly from the corresponding MCPT results depending on geometry and

TABLE III. Total macroscopic cross sections (cm^{-1}) for water, adipose tissue, and titanium, for each group of the three-group cross-section libraries.

Lib. name	Water ($\rho=1.0$ g cm^{-3})			Adipose tissue ($\rho=0.95$ g cm^{-3})			Ti ($\rho=4.54$ g cm^{-3})		
	Energy group			Energy group			Energy group		
	1	2	3	1	2	3	1	2	3
G-3a	0.4066	0.5101	10.759	0.3118	0.3725	2.641	27.099	37.418	1499
G-3b	0.4066	0.5101	10.759	0.3095	0.3693	6.493	26.246	38.258	218.38
G-3c	0.4139	0.5026	144.64	0.3137	0.3650	86.78	27.099	37.418	1499
G-3e	0.4151	0.7121	144.64	0.3144	0.4854	86.78	27.244	60.793	1499
G-3g	0.4068	0.4996	144.64	0.3095	0.3633	86.78	26,269	37.065	1499

TABLE IV. Group kerma factors ($\text{cm}^2 \text{g}^{-1}$) for water and adipose tissue for each group of the three-group cross-section libraries.

Lib. name	Water ($\rho=1.0 \text{ g cm}^{-3}$)			Adipose tissue ($\rho=0.95 \text{ g cm}^{-3}$)		
	Energy group			Energy group		
	1	2	3	1	2	3
G-3a	0.1662	0.3115	3.864	0.1027	0.1897	1.5312
G-3b	0.1662	0.3115	3.864	0.1014	0.1875	2.358
G-3c	0.1701	0.3068	31.53	0.1036	0.1847	19.66
G-3e	0.1708	0.4366	31.53	0.1040	0.2609	19.66
G-3g	0.1663	0.3046	31.53	0.1015	0.1835	19.66

material composition and the overall discrepancy relative to MCPT exceeds 5%. This finding is consistent with the G-3e group 2 cross section that differs significantly from the other three group values (Tables III and IV). The results are consistent with the observation in our previous work⁶ that source spectra do not constitute a suitable basis for deriving weighting functions.

Away from the Z axis DANTSYS simulations with the other three-group libraries closely approximate both the corresponding MCPT results and the DOM simulations based on the G-210 library. The relatively small (within 4%) discrepancies between DANTSYS simulations with G-3a to G-3g (excluding G-3e) that are evident from the figures, are due to the small relative differences in the respective cross sections discussed above (Tables III and IV). The results also demonstrate that when ^{125}I sources are used, the photon flux spectra are similar in all problems considered and this similarity holds for wide variations in geometry and material compositions. Larger discrepancies, generally exceeding 5%, are evident for all DANTSYS simulations within 5° of the Z axis. These differences increase with distance and with a decreasing number of angular directions and weights in the angular quadrature used. They are largely due to ray effects that are difficult to mitigate close to the axis of rotational symmetry.

The problem is also related to the particular implementation of the first collision source ray tracking technique in TWODANT and is discussed in detail in our previous work.^{1,6} We note that the volume exhibiting such larger errors constitutes less than 0.2% of the entire volume irradiated and therefore would have negligible impact on the accuracy of a volume-based modern treatment planning system. The large differences in the cross section data in group 3 (Tables III and IV) have a negligible impact on the calculations. Similar conclusions hold for all other distances studied.

To quantify the accuracy of DANTSYS simulations relative to MCPT in a compact form as a function of the cross-section library and other DOM operating parameters, we introduce the root mean square error (rms),

$$\text{rms}(\%) = \sqrt{\frac{1}{N} \sum_{k=1}^N \left(1 - \frac{\dot{D}_k^{\text{DANT}}}{\dot{D}_k^{\text{MCPT}}} \right)^2} \cdot 100, \quad (7)$$

where \dot{D}_k^{DANT} is the DANTSYS calculated absorbed dose rate per unit contained activity in the respective material at a point (r_k, θ_k) [Fig. 1(a)] and \dot{D}_k^{MCPT} is the corresponding MCPT value. N is the number of MCPT estimator points used in the comparison. It varies from problem to problem and is 141 for problems 1 and 2, 167 for problem 3 (air excluded),

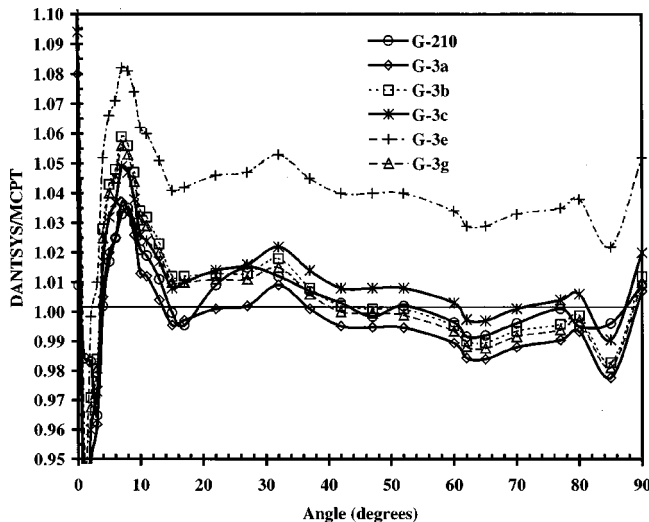


FIG. 5. Problem 1: DANTSYS absorbed dose rates in water relative to MCPT for angles θ in the range 0° – 90° at 1 cm from the seed center. S_{16} angular quadrature (36 angles and weights per octant). Various multigroup libraries.

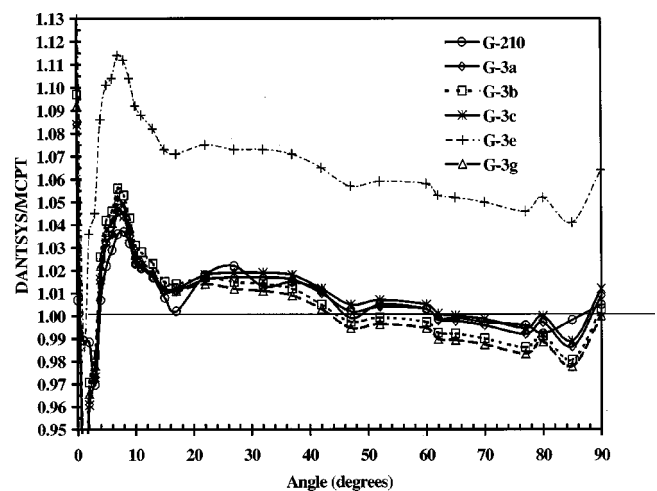


FIG. 6. Problem 2: DANTSYS absorbed dose rates in adipose tissue relative to MCPT for angles θ in the range 0° – 90° at 1.0 cm from the seed center. S_{16} angular quadrature (36 angles and weights per octant). Various multigroup libraries.

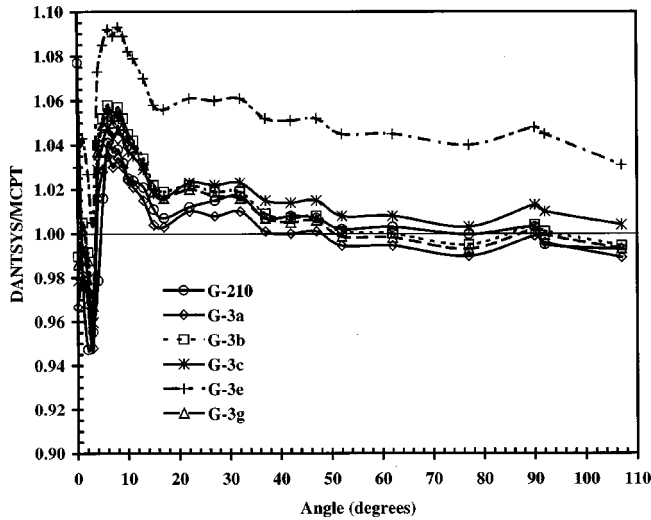


Fig. 7. Problem 3: DANTSYS absorbed dose rates in water relative to MCPT for angles θ in the range 0° – 96° at 1 cm from the seed center. S_{20} angular quadrature (55 angles and weights per octant). Various multigroup libraries.

and 253 in problem 4. To emphasize the differences due to the impact of each three-group library on the respective DANTSYS simulations and to minimize the influence of the ray effects, as discussed above, estimator points at θ_k in the range 0° – 4° , 176° – 180° , from the Z axis at all distances are excluded from rms values evaluated by Eq. (7). Table V gives these values as a function of the angular quadrature and multigroup library used in the calculations for each problem. For comparison, the table also includes the results with G-210.

Table V shows that DANTSYS simulations with G-210 consistently lead to rms values of less than or about 2.1% for all angular quadratures used except for problems 3 and 4, where the use of S_{16} produces rms estimates bigger than 2.5%. The larger number of voxels in problems 3 and 4, needed to accurately represent the photon leakage through the water–

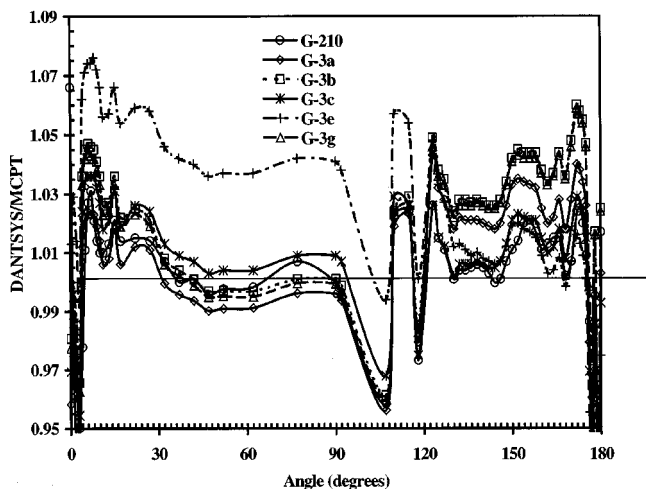


Fig. 8. Problem 4: DANTSYS absorbed dose rates in water relative to MCPT for angles θ in the range 0° – 180° at 1.0 cm from the seed center. S_{20} angular quadrature (55 angles and weights per octant). Various multigroup libraries.

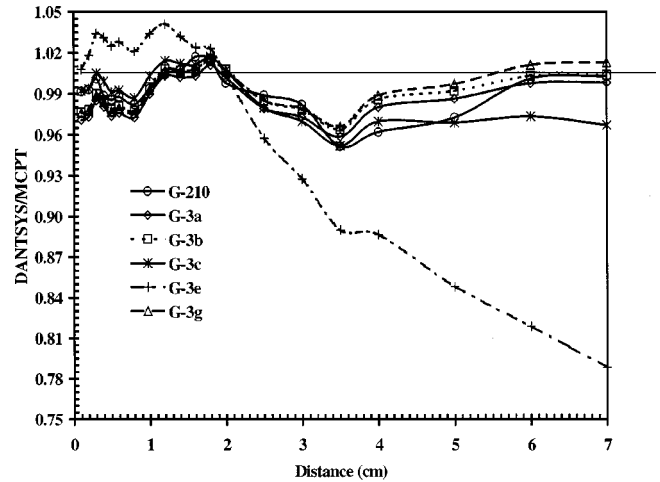


Fig. 9. Problem 4: DANTSYS absorbed dose rates in water relative to MCPT for distances r in the range 0.1–7 cm along the seed traverse plane ($\theta=90^\circ$). S_{20} quadrature (55 angles and weights per octant). Various multigroup libraries.

air interface (problem 3) or the attenuation of the iron disk (problem 4), required more angular directions for the discretization of the angular variable for better accuracy. Further, simulations with G-3e lead to distinctly larger rms errors that exceed the corresponding G-210 estimates by a factor of 4 or more for all problems. This result, consistent with Figs. 5–9, indicates the unsuitability of the I-125 primary photon spectrum as a weighting function. Overall, simulations with the three-group libraries result in larger rms values than with G-210. However, it is evident that G-3a and G-3c calculations closely approximate those with G-210. Both G-3a and G-3c lead to rms values of less than 2.5% for all problems and angular quadratures except for S_{16} and problems 3 and 4, consistent with G-210. At the same time, rms estimates for G-3b and G-3g exceed 2% in all cases and increase faster with a decreasing number of directions and weights used in the angular quadrature.

The successful implementation of both G-3a and G-3c indicates the following.

- (1) Material-specific weighting functions (G-3a) results in accurate DOM absorbed dose-rate calculations for ^{125}I sources over a broad range of heterogeneous geometries.
- (2) At least in the case of the model 6702 seed, equivalent accuracy can be achieved using a single material-independent weighting function (G-3c) based upon the photon spectrum in Ti.

However, even relatively small variations in the cross sections (Tables III and IV) due to the weighting function may cause distinct deterioration in the accuracy, as seen with G-3b and G-3g. This indicates that the most appropriate weighting function (or set of weighting functions) is not obvious and cannot be derived without extensive analysis of the related radiation transport problems. The implementation of DANTSYS with a fine multigroup energy structure proves to be a useful and efficient tool in deriving and validating broad multigroup libraries.

TABLE V. The rms values for various libraries and problems 1–4 for angular quadrature sets S_{36} (171 angular directions and weights), S_{30} (120 directions and weights), S_{26} (91 directions and weights), S_{20} (55 directions and weights), and S_{16} (36 directions and weights). Absorbed dose rates in water only evaluated in problems 1, 3, and 4. Both dose rates in water and adipose tissue evaluated in problem 2. Estimator points for angles θ in the range 0° – 4° , 176° – 180° with respect to the Z axis are excluded (see the text). The 141 Monte Carlo estimator points used in problems 1 and 2; 167 in problem 3 (air excluded); and 253 in problem 4.

	Library	S_{36}	S_{30}	S_{26}	S_{20}	S_{16}
Problem 1	G-210	1.11	1.07	1.25	1.51	1.76
	G-3a	1.59	1.65	1.67	1.84	2.44
	G-3b	2.06	2.15	2.15	2.39	3.06
	G-3c	1.54	1.65	1.67	1.84	2.39
	G-3g	2.20	2.28	2.28	2.52	3.21
	G-3e	9.50	9.55	9.56	9.50	9.33
Problem 2	G-210	1.26	1.24	1.40	1.70	2.10
	G-3a	1.28	1.40	1.45	1.69	2.17
	G-3b	2.05	2.12	2.13	2.40	2.96
	G-3c	1.48	1.57	1.61	1.86	2.32
	G-3g	2.16	2.22	2.23	2.51	3.10
	G-3e	9.22	9.28	9.29	9.26	9.11
Problem 3	G-210	1.38	1.41	1.60	2.04	2.70
	G-3a	1.69	1.67	1.73	2.24	2.67
	G-3b	2.28	2.28	2.35	2.87	3.31
	G-3c	1.82	1.80	1.93	2.43	2.80
	G-3g	2.30	2.30	2.36	2.89	3.35
	G-3e	7.33	7.31	7.39	7.42	7.31
Problem 4	G-210	1.39	1.40	1.49	2.07	2.55
	G-3a	1.96	1.99	2.08	2.55	3.02
	G-3b	2.78	2.82	2.94	3.42	3.89
	G-3c	1.95	1.97	2.02	2.39	2.76
	G-3g	2.89	2.93	3.05	3.56	4.03
	G-3e	11.0	11.0	11.0	10.8	10.7

We used Table V results to select the most appropriate angular quadrature for comparing the computational efficiency of DOM and Monte Carlo calculations. We note that the “best” angular and spatial discretization scheme is a complicated function of geometry and other physical proper-

ties of the modeled system and its choice cannot be made *a priori*.² Therefore, we assumed that the spatial discretization is already made (as described in Sec. II C) and only the angular quadrature is to be selected. As an accuracy criterion, we sought the lowest-order problem-dependent angular quadrature for which the following conditions are true simultaneously: the rms value of the DANTSYS G-210 simulation does not exceed 2.1%; the rms value of DANTSYS with G-3a or G-3c does not exceed 2.5%.

From Table V it is clear that S_{16} for problems 1 and 2, and S_{20} for problems 3 and 4 satisfy these conditions. These considerations were used to justify the selection of S_{16} and S_{20} results shown in Figs. 3 and 5–9. We note that the use of G-3b or G-3g with the conditions above would require higher-order quadratures (S_{20} and S_{26} , respectively) which reduces the efficiency.¹

Table VI compares the CPU run times of DANTSYS and EGS4²¹ simulation using identical mesh-based geometries and scoring grids. The “iterations CPU time” is the time used for the actual discrete ordinates solution only, while the total CPU time includes time spent in calculating the first collision source as well. All times are valid on our SGI RS10000 workstation. The data indicates that DANTSYS calculations with the three-group libraries can produce gains in efficiency, generally exceeding a factor of 80. When only the CPU time consumed by DOM iterations is considered, gain factors exceeding 300-fold results. This large discrepancy in efficiency (by a factor of 3) is due to the large fraction of the overall CPU time (up to 75%) used for first collision source calculations. As discussed previously,^{1,6} the TWODANT ray-tracing first-collision source does not efficiently calculate collision density distributions around brachytherapy sources. The relatively simple source geometry typical of brachytherapy problems (at least relative to the reactor physics problems for which DANTSYS was originally designed), however, suggests the approximations of the exact ray tracing used by DANTSYS’s first collision source, may have the potential of im-

TABLE VI. Total CPU times (min) and iteration CPU time (min) needed for DANTSYS with S_{16} (36 angles and weights per octant) for problems 1 and 2, and S_{20} (55 angles per octant) for problems 3 and 4, and various multigroup libraries, a comparison with the EGS4 2D Monte Carlo code DOSRZ. DOSRZ is run until the standard deviation (SD%) in 99% of the phantom volume reached the values shown. In problem 3 only 99% of the water fraction of the overall phantom is accounted for. All times are valid on a SGI RS10000 workstation. EGS4 CPU times for problems 1 and 2 are reduced by a factor of 2 to account for the reflection boundary condition applied in the related DANTSYS calculations along the source transverse plane.

	DANTSYS													EGS4/DOSRZ	
	G-210				G-3a				G-3c				Number of histories (millions)	SD%	CPU (min)
	# iterations	Total CPU (min)	Iterations CPU (min)	Total EGS4/DANTSYS CPU	# iterations	Total CPU (min)	Iterations CPU (min)	Total EGS4/DANTSYS CPU	# iterations	Total CPU (min)	Iterations CPU (min)	Total EGS4/DANTSYS CPU			
Problem 1 (S_{16})	375	37	29	9	15	4.5	1.1	71	16	4.4	1.1	73	230	2.6	321
Problem 2 (S_{16})	387	38	29	10	16	4.4	1.1	86	16	4.4	1.1	86	240	2.4	378
Problem 3 (S_{20})	388	122	101	10	18	9.9	4.3	125	17	9.5	4.1	130	400	2.8	1238
Problem 4 (S_{20})	384	125	102	5	15	9.3	3.7	62	16	9.3	3.8	62	220	2.8	573

proving efficiency without loss of accuracy (e.g., the non-parametric “nearest pixel” ray-tracing algorithm²⁵).

However, Table VI shows that even with the current first collision source algorithm, the three-group libraries require run times of less than 10 min on our SGI RS 10000 workstation. The three-group DANTSYS calculations are a factor of 10–13 faster than the corresponding G-210 simulations. If the iterations CPU time is compared only, however, the gain exceeds a factor of 25, indicating that as the energy group number is reduced, the ray-tracing first collision source calculation requires a larger fractions of the overall CPU time. The reduction in DOM iterations CPU time is due to the reduced (28-fold) number of energy groups used in the problems’ solution. The use of higher-order spatial-differencing schemes²⁶ and/or Adaptive Mesh Refinement (under development in Los Alamos National Laboratory) is expected to allow the use of larger voxel sizes, reducing the number of spatial mesh cells, and further enhancing efficiency.

It must be emphasized that these efficiency gains are valid only in comparison to DOSRZ/EGS4 Monte Carlo simulations in two-dimensional R-Z geometry using simple analog¹² scoring. By using more sophisticated estimators and advanced variance reduction methods, significantly improved Monte Carlo performance can be achieved, thus reducing the efficiency advantage of DOM. In addition, the observed gains may not be sustained in more complex three-dimensional geometries. Nevertheless, our results suggest that discrete ordinates-based dose calculation may be competitive with Monte Carlo simulations and do appear to outperform dimensionally and geometrically matched conventional analog MC simulations. This conclusion is consistent with the conclusions of the analysis by Börger²⁷ and demonstrates that the use of second-order spatial and angular differencing schemes (AWDD in DANTSYS) may lead to significant efficiency gain. We consider these results very encouraging and are currently evaluating the accuracy and efficiency of full three-dimensional DOM simulations.

IV. CONCLUSIONS

The DANTSYS discrete ordinates system with the high-energy resolution 210-group cross-section library has been used to obtain spectral weighting functions for use with a model 6702 ¹²⁵I seed in a broad range of heterogeneous geometries.

The obtained broad three-group libraries, strictly speaking, are applicable only to geometries, radionuclides, and spatial cells from which these spectral weighting functions were derived. However, in the study we demonstrate that a single precalculated three-group library, derived from spectral distributions at only a few points in the geometry, maintains dose-calculation accuracy within 3%–5% relative to Monte Carlo over a broad range of ¹²⁵I brachytherapy problem geometries.

The broad-group DANTSYS calculations were 10- to 13-fold faster than G-210 simulations and as much as 125-fold faster than the geometrically matched EGS4 analog Monte Carlo simulations. However, the current DANTSYS first-

collision source routine significantly limits the efficiency gains achievable. The current developments in deterministic transport simulations, e.g., nonlinear differencing schemes and locally recursive spatial grids, may allow for even larger future gains.

The study presented is by no means exhaustive. We made no attempt to obtain an optimal (in a sense of either accuracy or efficiency) energy group structure and weighting functions or finite-difference grid representation of the geometry. The reported efficiency gains were obtained for two-dimensional problems. Future studies are needed to demonstrate that both the accuracy and efficiency gains achieved can be sustained in three-dimensional geometries. However, the results strongly support the hypothesis that deterministic solutions of the linear Boltzmann transport equations, which have been largely neglected by the radiotherapy community, have significant potential as a treatment planning tools for brachytherapy and other treatment modalities utilizing low-energy photon fields.

ACKNOWLEDGMENT

The present study was supported by the National Institutes of Health Grant No. R01 CA46640.

^aCorresponding author. Phone: (613)-993-2715; Fax: (613)-952-9865; Electronic mail: daskalov@irs.phy.nrc.ca

¹G. M. Daskalov, R. S. Baker, D. W. O. Rogers, and J. F. Williamson, “Dosimetric modeling of the microSelection high-dose rate ¹⁹²Ir source by the multigroup discrete ordinates method,” *Med. Phys.* **27**, 2307–2319 (2000).

²E. E. Lewis and W. F. Miller, Jr., *Computational Methods of Neutron Transport* (Wiley, New York, 1984).

³J. F. Williamson, “Recent development in basic brachytherapy physics,” in *Radiation Therapy Physics*, edited by A. R. Smith (Springer-Verlag, Berlin, 1995), pp. 247–302.

⁴J. F. Williamson, H. Perera, Z. Li, and W. R. Lutz, “Comparison of calculated and measured heterogeneity correction factors for ¹²⁵I, ¹³⁷Cs, and ¹⁹²Ir brachytherapy sources near localized heterogeneities,” *Med. Phys.* **20**, 209–222 (1993).

⁵G. M. Daskalov, R. S. Baker, R. C. Little, D. W. O. Rogers, and J. F. Williamson, “Multigroup discrete ordinates photon transport calculations of water kerma for brachytherapy applications,” in the *Proceedings of the ANS Topical Conference*, 19–23 April 1998, Nashville, TN, Vol. 2, pp. 261–268.

⁶G. M. Daskalov, R. S. Baker, R. C. Little, D. W. O. Rogers, and J. F. Williamson, “Two dimensional discrete ordinates photon transport calculations for brachytherapy dosimetry applications,” *Nucl. Sci. Eng.* **134**, 121–134 (2000).

⁷R. E. Alcouffe, R. S. Baker, F. W. Brinkley, D. R. Marr, R. D. O’Dell, and W. F. Walters, DANTSYS: A Diffusion Accelerated Neutral Particle Transport Code System,” LA-12969-M, Los Alamos National Laboratory, Los Alamos, NM, June 1995.

⁸International Commission on Radiation Units and Measurements Report ICRU 60, “Fundamental quantities and units for ionizing radiation,” Bethesda, MD, 1998.

⁹R. E. MacFarlane and D. W. Muir, “The NJOY nuclear data processing system version 91,” LA-12740-M, Los Alamos National Laboratory, Los Alamos, NM, 1994.

¹⁰R. Nath, L. L. Anderson, G. Luxton, K. A. Weaver, J. F. Williamson, and A. S. Meigooni, “Dosimetry of interstitial brachytherapy sources: Recommendations of the AAPM Radiation Committee Task Group No. 43,” *Med. Phys.* **22**, 209–234 (1995).

¹¹R. K. Valicenti, A. S. Kirov, A. S. Meigooni, V. Mishra, R. K. Das, and J. F. Williamson, “Experimental validation of Monte Carlo dose calcula-

- tions about a high-intensity Ir-192 source for pulsed dose-rate brachytherapy," *Med. Phys.* **22**, 821–829 (1995).
- ¹²J. F. Williamson, "Monte Carlo evaluation of kerma at a point for photon transport problems," *Med. Phys.* **14**, 567–576 (1987).
- ¹³J. F. Williamson and Z. Li, "Volume-based geometric modeling for radiation transport calculations," *Med. Phys.* **19**, 667–678 (1992).
- ¹⁴J. F. Williamson, Z. Li, and H. Perera, "Monte Carlo calculation of kerma-to-a-point in the vicinity of media interfaces," *Phys. Med. Biol.* **38**, 1825–1840 (1993).
- ¹⁵G. M. Daskalov, E. Loffler, and J. F. Williamson, "Monte Carlo-aided dosimetry of a new high dose-rate brachytherapy source," *Med. Phys.* **25**, 2200–2208 (1998).
- ¹⁶RSIC Data Library DLC-146, "HUGO-VI: Photon Interaction Data in ENDF/B-VI Format," RSICC, ORNL, Oak Ridge, TN, August 1989.
- ¹⁷J. H. Hubbell and S. M. Seltzer, "Tables of x-ray mass attenuation coefficients and mass energy-absorption coefficients 1 keV to 20 MeV for elements Z=1 to 92 and 48 additional substances of dosimetric interest," NISTIR 5632, May 1995.
- ¹⁸F. H. Attix, *Introduction to Radiological Physics and Radiation Dosimetry* (Wiley, New York, 1986).
- ¹⁹J. F. Williamson, "The Sievert integral revisited: Evaluation and extension to ¹²⁵I, ¹⁶⁹Yb, and ¹⁹²Ir brachytherapy sources" *Int. J. Radiat. Oncol., Biol., Phys.* **36**, 1239–1250 (1996).
- ²⁰NCRP Report No. 58, *A Handbook of Radioactivity Measurements Procedures*, 2nd ed. (National Council of Radiation Protection, Washington, DC, 1985).
- ²¹W. R. Nelson, A. Hirayama, and D. W. O. Rogers, "The EGS4 code system," Stanford Linear Accelerator Center Report SLAC-265, Stanford, CA 1985.
- ²²R. E. Alcouffe, "An adaptive weighted diamond differencing method for three-dimensional XYZ geometry," *Trans. Am. Nucl. Soc.* **68A**, 206–208 (1993).
- ²³R. E. Alcouffe, "Diffusion synthetic acceleration methods for the diamond-differencing discrete-ordinates equations," *Nucl. Sci. Eng.* **64**, 344–355 (1977).
- ²⁴R. S. Baker, "A stochastic first collision source for TWODANT," in the *Proceedings of the 8th International Conference on Radiation Shielding*, 1994, Arlington, TX, Vol. 1, pp. 157–164.
- ²⁵M. W. Frandsen, D. E. Wessol, F. J. Wheeler, R. S. Babcock, G. H. Harkin, and J. D. Starkey, "Rapid interrogation for a uniform volume element-based Monte Carlo particle transport simulations," in the *Proceedings of the ANS Topical Conference*, 19–23 April 1998, Nashville, TN, Vol. 2, pp. 84–94.
- ²⁶R. D. O'Dell and R. E. Alcouffe, "Transport calculations for nuclear reactors," in the *CRC Handbook of Nuclear Reactor Calculations*, edited by Y. Ronen (CRC, Boca Raton, FL, 1986), Vol. I, pp. 341–462.
- ²⁷C. Börgers, "Complexity of Monte Carlo and deterministic dose-calculation methods," *Phys. Med. Biol.* **43**, 517–528 (1998).